

QUANTIFICATION OF NUMERICAL AND MODEL UNCERTAINTIES IN THE CFD SIMULATION OF THE GAS HOLDUP AND FLOW DYNAMICS IN A LABORATORY SCALE RUSHTON-TURBINE FLOTATION TANK

Mohsen KARIMI^{*1}, Guven AKDOGAN¹, Kiran H. DELLIMORE², Steven M. BRADSHAW¹

¹ Department of Process Engineering, Stellenbosch University, Private Bag X1 Matieland 7602, Stellenbosch, South Africa.

² Department of Mechanical and Mechatronic Engineering, Stellenbosch University, Private Bag X1 Matieland 7602, Stellenbosch, South Africa.

*Corresponding author: Mohsen Karimi, E-mail address: karimi@sun.ac.za

ABSTRACT

The gas holdup and flow dynamics in a laboratory scale Rushton-turbine flotation tank were simulated using the dispersed k- ϵ turbulence model and Eulerian-Eulerian multiphase modelling approach. The inherent uncertainties in the CFD predictions were quantified by examining the model and numerical (i.e., discretization) uncertainties. The contribution of model uncertainty was explored by considering different sparger geometries while numerical uncertainty was evaluated using the Grid Convergence Index (GCI). The numerical predictions of the gas holdup for different sparger configurations showed that sparger design and location can have a significant impact on the results. Numerical uncertainty was found to be less significant since the average GCI value was less than 11.7%, for the numerical predictions of the velocity components and the turbulence parameters. Overall, the results suggest that quantification of uncertainties in CFD simulations can lead to improved predictions of the gas holdup and flow dynamics in a laboratory scale Rushton-turbine tank.

NOMENCLATURE

C_D	drag coefficient
d	bubble diameter
E_1^{fine}	fractional error for the fine grid solution
f_{1-3}	solutions for fine, medium and coarse mesh
F_d	drag force
\vec{F}_{lift}	lift force
\vec{F}_q	external body force
F_S	Safety factor
\vec{F}_{vm}	virtual mass force
\vec{g}	gravity vector
GCI	Grid Convergence Index
h	height
H	tank height
h_{1-3}	grid spacing for fine, medium, and coarse mesh
I	unit vector
p	formal order of accuracy of the algorithm
r	grid refinement ratio
Re	Reynolds number
\vec{R}_{pq}	interfacial force
S_q	mass source term
t	time
\vec{U}_q	mean velocity vector

y^+	dimensionless wall distance
α_q	volume fraction of phase q
ϵ	relative error
λ	turbulent viscosity
μ	laminar viscosity
ρ	density

INTRODUCTION

The standard Rushton-turbine flotation tank is a mechanically stirred mixer widely used in mineral processing plants to perform standard operations such as solid suspension, and gas dispersion. The uniform dispersion of gas in the flotation tank is of importance, as it provides an appropriate environment for the air bubbles and the solid particles to collide and attach to ensure effective separation in the flotation process. In order to determine the homogeneity of the gas phase within an agitated tank many attempts have been made to correlate the gas holdup with the geometrical and operational parameters of the stirred tank. For instance, Sensel et al. (Sensel et al., 1992) proposed an empirical equation for the gas holdup based on the three dimensionless numbers including the air flow number, Froude number and Reynolds number. In another attempt, Finch et al. (Finch et al., 2000) suggested a linear formulation between the gas holdup and the bubble surface area flux. However, these correlations do not provide physical insight into the underlying hydrodynamics of the flow and they are case dependent. Therefore, it is important to study the physics of the flow inside the stirred tank to gain detailed information for the design and optimization of the actual process conditions.

Computational Fluid Dynamics (CFD) offers an alternative to empirical correlations. It can simulate the flow inside the stirred tank through the numerical solution of the equations governing the flow hydrodynamics. One of the first studies on the numerical modelling of the stirred tank was performed by Dong et al. (Dong et al., 1994a, Dong et al., 1994b). They measured the velocity components using LDV and applied these experimental data to validate their numerical predictions. They showed a satisfactory agreement between the predictions and the measurements in the bulk flow, while in the impeller region the disagreement between the CFD solution and the experiments was attributed to the high turbulent intensity in this zone. Using the multiple reference frames (MRF) method Oshinowo et al. (Oshinowo et al., 2000) predicted the tangential velocity distribution in a baffled tank. They

suggested that the MRF method is useful for the design and analysis of the single phase and turbulent flow inside the stirred tank. In the same year, Lane et al. (Lane et al., 2000) compared the MRF and the sliding mesh methods for the single phase modelling of the stirred tank. They also confirmed that for the same level of numerical accuracy, the MRF method is more economical than the sliding mesh approach. In follow-up studies (Lane et al., 2002, Lane et al., 2005) they predicted the gas-liquid flow in the mechanically stirred tank using an Eulerian-Eulerian method to model the multiphase flow. They proposed a new correlation for the drag coefficient in which the interaction of the air bubbles with the turbulent eddies was considered. They showed that the predictive capability of the CFD model was improved by including the effect of turbulence on the drag force. Kerdouss et al. (Kerdouss et al., 2006) also performed an Eulerian-Eulerian simulation in conjunction with the k- ϵ turbulence model to predict the gas dispersion and the bubble size distribution in a double turbine stirred tank. A bubble number density equation was implemented to account for the combined effect of the bubble break-up and coalescence. The predicted distribution of the gas phase and the average local bubble size were in good agreement with the experimental data from the literature. Recently, the numerical challenges associated with the CFD simulation of the stirred tank were discussed by Coroneo et al. (Coroneo et al., 2011). They emphasized that one of the major factors limiting the accurate numerical prediction of the flow within a stirred tank is uncertainty (i.e. mesh size and discretization schemes) for single phase and multiphase modelling.

The accuracy of CFD predictions is commonly evaluated by comparing the predictions with experimental data. In this approach the error is simply computed as the percentage of difference between the predictions and measurements. However, the inherent errors and uncertainties in the numerical predictions themselves are not considered. It is therefore important to be able to quantify these uncertainties with a systematic method to enhance the level of confidence in the predictions.

While many approaches have been devised through the years for reporting the uncertainty in numerical simulations, the method proposed by Roache (Roache, 1994) is the most widely accepted. Roache suggested a systematic way of reporting the grid convergence studies and numerical errors using the Grid Convergence Index (GCI). In order to assess the influence of discretization and iterative convergence errors the GCI compares the discrete solutions at two different grid spacing.

The aim of this paper is to investigate and to quantify the uncertainties in the CFD modelling of the stirred tank. The systematic method of GCI is applied to evaluate the impact of numerical uncertainty on the CFD predictions.

METHODOLOGY

One of the key requirements before simulating the flow inside the stirred tank is to understand the origins of uncertainties in the numerical solutions. Freitas (Freitas, 2002) classified the uncertainties in numerical simulations into three different categories: (a) input uncertainty, which arises from the input parameters such as the hydrodynamics properties of water and air, (b) model uncertainty, which occurs due to the different formulations, structure and implementations, and (c) numerical uncertainty which accounts for the effect of discretization and iterative errors. Of the three types of uncertainties, the input and model uncertainties can be

eliminated by the specification of the input parameters with a high level of accuracy and by using enhanced models or codes. In the latter case, however, some model uncertainty is always present in the numerical simulations. Thus, it is important to identify and quantify the numerical uncertainty in CFD simulations to provide an error bound. In this paper the numerical uncertainty was quantified using the Grid Convergence Index (GCI) proposed by Roache (Roache, 1994). The GCI method is based on the generalized theory of Richardson extrapolation (Richardson, 1911, Richardson and Gaunt, 1927). In order to perform the GCI test three different grids spacing, h_1 , h_2 , and h_3 yielding three solutions, f_1 , f_2 , and f_3 for the fine, medium and coarse mesh resolutions are required. The first step in computing the GCI is to calculate the fractional error for the fine grid solution (f_i) as follows:

$$E_1^{fine} = \frac{\epsilon}{1-r^p} \quad (1)$$

where the relative error is $\epsilon = (f_2 - f_1)/f_1$, r equals the grid refinement ratio (i.e., h_2/h_1), and p is the formal order of accuracy of the algorithm, which is given by:

$$p = \frac{\ln\left(\frac{f_3 - f_2}{f_2 - f_1}\right)}{\ln r} \quad (2)$$

where f_1 , f_2 , and f_3 are the solutions for fine, medium and coarse mesh schemes, respectively.

Roache defined the GCI as a scale to evaluate how far the solution is from the asymptotic value and highlighted that a small value of GCI is an indication that the numerical uncertainty due to the discretization error is negligible. The GCI for the fine solution can be written as:

$$GCI_{fine} = \frac{F_s |\epsilon|}{(r^p - 1)} \quad (3)$$

where F_s is a safety factor. Roache recommended a range of $1.25 \leq F_s \leq 3$ for the safety factor. Depending on the required accuracy, one can select the magnitude of this factor. A higher F_s can be chosen if a more conservative level of confidence in the CFD predictions is desired.

NUMERICAL APPROACH

The turbulent flow of the liquid-gas inside a 145 mm diameter stirred tank, based on the geometry of Newell (Newell and Grano, 2007), was modelled using an Eulerian multiphase model. The governing continuity and momentum equations which were solved for each phase, q , can be expressed as follows:

$$\frac{\partial}{\partial t}(\alpha_q \rho_q) + \nabla \cdot (\alpha_q \rho_q \vec{U}_q) = S_q \quad (4)$$

$$\frac{\partial}{\partial t}(\alpha_q \rho_q \vec{U}_q) + \nabla \cdot (\alpha_q \rho_q \vec{U}_q \vec{U}_q) = -\alpha_q \nabla p + \alpha_q \rho_q \vec{g} + \nabla \cdot (\alpha_q \mu_q (\nabla \vec{v}_q + \nabla \vec{v}_q^T)) + \alpha_q \left(\lambda_q - \frac{2}{3} \mu_q \right) \nabla \cdot \vec{v}_q \mathbf{I} + \sum_{p=1}^n \vec{R}_{pq} + \vec{F}_q + \vec{F}_{lift} + \vec{F}_{vm} \quad (5)$$

where α_q is the volume fraction of phase q , ρ_q is the density, \vec{U}_q is the mean velocity vector, S_q is the mass source term (e.g. a source of air at the sparger), p is the pressure, \vec{g} is the gravity vector, μ_q is the laminar viscosity, λ_q is the turbulent viscosity, \mathbf{I} is the unit vector, \vec{R}_{pq} is the interfacial force, \vec{F}_q is the external body force, \vec{F}_{lift} is the lift force, and \vec{F}_{vm} is the virtual mass force.

Previous work has shown that the dominant interfacial force term in the gas-liquid flow of stirred tanks is the drag force (Khopkar et al., 2006, Kerdouss et al., 2006, Lane et al., 2002). In this paper the influence of the drag force was included using the standard Schiller-Naumann drag correlation (Schiller and Naumann, 1935), while the

other forces were assumed to be insignificant. The drag force can be written as follows:

$$F_d = \frac{3}{4} \rho_l \alpha_g \frac{C_D}{d} |\vec{U}_g - \vec{U}_l| (\vec{U}_g - \vec{U}_l) \quad (6)$$

Here, the subscript l and g represent the liquid and the gas phases, d is the bubble diameter, and C_D is the drag coefficient which was computed using the standard Schiller-Naumann correlation:

$$C_D = \begin{cases} \frac{24(1+0.15Re^{0.687})}{Re} & Re \leq 1000 \\ 0.44 & Re > 1000 \end{cases} \quad (7)$$

where Re is the relative Reynolds number for the bubbles:

$$Re = \frac{\rho_l |\vec{U}_g - \vec{U}_l| d}{\mu_l} \quad (8)$$

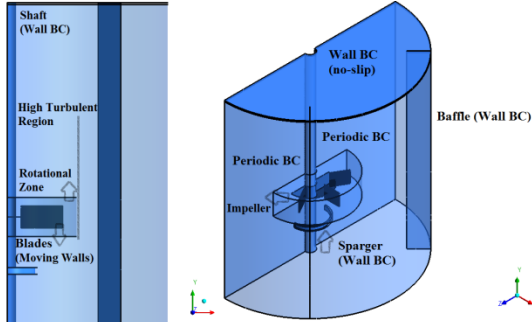


Figure 1: Schematic illustration of boundary conditions. Figure 1 shows the boundary conditions used in this paper. The multiple reference frames (MRF) method was implemented to model the rotation of the impeller. To apply the MRF method, the entire vessel was divided into two regions, the bulk zone where the governing equations were solved in a stationary reference frame, and the rotational zone where the flow was calculated in a rotating reference frame. To minimize the uncertainties associated with the size of the rotational zone, preliminary tests were performed to determine the appropriate extent of the rotational zone around the impeller. From these tests it was found that a zone with dimensions of $1.376 \text{ blade heights} \times 1.125 \text{ impeller diameters}$ gave the best agreement with the experimental data of Newell (Newell, 2006) (Figure 1). Moving wall boundary conditions were prescribed for the blades inside the rotational zone (i.e., the angular velocity of zero relative to the rotational zone). In addition, the sparger was modelled using a wall boundary condition and a mass source of air with a constant bubble size as reported by Newell. This was done in order to mimic the sparging of air into the vessel. Since the geometry of the stirred tank used in this study is rotationally symmetric the computational domain was limited to half of the tank and periodic boundary conditions were applied. The remaining boundaries including the baffles and the tank walls were set as no slip velocity boundary conditions.

All the simulations were performed on a High Performance Computing (HPC) cluster with 8 nodes and an installed capacity of 2.83GHz processors per node with 16GB of RAM. ANSYS Fluent was used to solve the governing equations. To derive the pressure field inside the tank, the SIMPLE scheme was used to couple the continuity and momentum equations. A second order upwind discretization method was used for the momentum equations, while the volume fraction equation was computed using the QUICK method. The solution was considered converged when the normalized continuity residuals were less than 1×10^{-3} and the variations in the predicted gas holdup were negligible (i.e., a difference of

less than 1% between the final gas holdup value and the average value for the last five seconds of the flow time).

The input uncertainties were minimized by specifying all the input constants and parameters with a high level of precision (to six significant digits). A turbulence model study was performed in order to reduce the influence of model uncertainty in the numerical predictions. The results showed that the dispersed k- ϵ model yielded better prediction of the flow (Karimi et al., 2012).

The GCI test was carried out to quantify the numerical uncertainty. Three structured hexagonal mesh schemes with a constant grid refinement ratio of two were generated (Table 1). The quality of each mesh was examined by the skewness ratio. Also, to capture the temporal turbulent fluctuations the maximum y^+ (i.e., the dimensionless wall distance) was kept within the logarithmic law layer in all cases (i.e., $30 < y^+ < 300$).

Mesh	Type	Size interval (mm)	No. of cells	% cells with skewness < 0.2	CPU time (h)
Coarse	Hex	4	65,723	92.24	0.2
Medium	Hex	2	476,010	96.61	2.1
Fine	Hex	1	3,744,472	94.90	77.6

Table 1: Mesh properties

RESULTS AND DISCUSSION

Quantification of model uncertainty

To minimize the effects of model uncertainties in the numerical predictions of the gas holdup two types of sparger designs (i.e., disk and ring configurations) with three diameters (d_s) are explored. The sparger diameters are chosen based on the impeller diameter (D). In addition, each sparger design is located at three different distances from the impeller to investigate the influence of the sparger location on the gas holdup. In order to introduce the gas into the cell, the source term is defined at the sparger injecting the gas with the same flow rate as in the experimental data (Table 2, Figure 2, and Appendix 1).

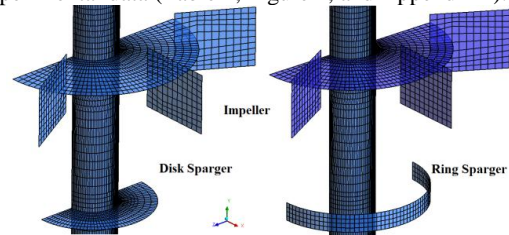


Figure 2: Schematic diagram of the ring and disk spargers. The CFD predictions of the gas holdup are validated by comparison to experimental data from Newell which was 5.2% for angular velocity of 350rpm (Newell, 2006). It is important to note the gas holdup measurement of Newell was acquired using a porous plate for the sparger. Simulation of this did not yield a converged solution, as the small gas velocity related to the large sparger area created numerical uncertainties. The predicted gas holdup (i.e., volume weighted average of the gas volume fraction) for all the sparger designs are summarized in Table 2.

Type	d_s/D	Angular velocity (rpm)	Predicted gas holdup (%)
Ring	0.50	350	4.33
Ring	0.75	350	4.81
Ring	1.0	350	5.63
Disk	0.40	350	6.86
Disk	0.50	350	14.6
Disk	0.75	350	36.6

Table 2: Gas holdup for different sparger designs

The results in Table 2 clearly show that sparger design significantly influences the gas holdup predictions. The comparison of the ring and the disk sparger demonstrates that the ring designs predict the gas holdup closer to the experimental data within an average difference of 10.8%. Also, for both designs increasing the diameter results in an increase for the gas holdup predictions. However, using a large diameter ($d_s/D > 0.4$) disk sparger leads to an unrealistic gas holdup value. The reason for the observed phenomenon can be explained by the fact that the gas velocity is reduced by increasing the cross sectional area of the sparger to maintain a constant gas flow rate. Therefore, the gas phase has more time to accumulate behind the blades and baffles thereby increasing the overall volume fraction of gas in the tank.

As mentioned three different locations for the sparger were also considered: at the bottom of the tank, at the middle of clearance, and near to the impeller.

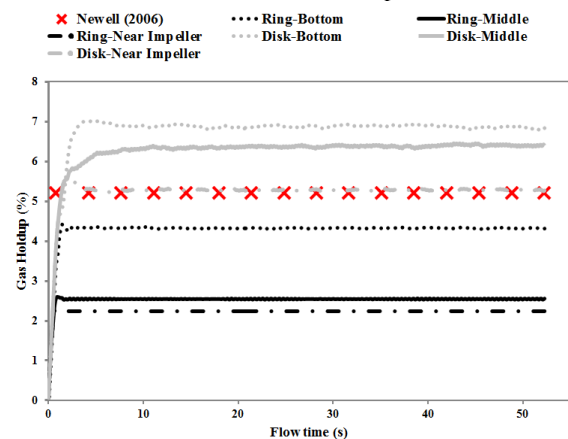


Figure 3: Gas holdup as a function of flow time for two different sparger designs at three different locations.

To verify that the effects of model uncertainty were minimized, the gas holdup predictions for three different sparger positions were compared in Figure 3. The figure shows the predicted gas holdup as a function of flow time. The symbols indicate the experimental data of Newell, the solid lines correspond to the predictions for the sparger at the middle of the clearance (i.e., the impeller distance from the bottom of the tank), the dashed lines to predictions for the sparger close to the impeller, and the dotted lines to predictions for sparger at the bottom of the tank. Two different colours, grey and black, were also used to display the disk and ring sparger designs, respectively. The results show that the position of the sparger can significantly vary the numerical predictions. The predicted values of the gas holdup for the both designs decrease when the sparger approaches the impeller. The disk sparger in different positions over predicts the gas holdup to within an average difference of 32.0%, 23.3%, and 1.5% for the sparger at the bottom, the middle of clearance, and close to the impeller, respectively. However, the computed gas holdup values for the ring design have been underpredicted to within an average difference of 16.8%, 50.9, and 56.9% for the locations of sparger at the bottom, the middle of clearance, and close to the impeller, respectively. Based on these results it can be concluded that sparger design and location can significantly influence the numerical predictions of the gas holdup in a stirred tank. This suggests that in order to improve confidence of the gas holdup predictions, quantification of the model uncertainties due to the sparger

designs, which have not been reported previously, should be accounted for in the CFD methodology.

Quantification of numerical uncertainty

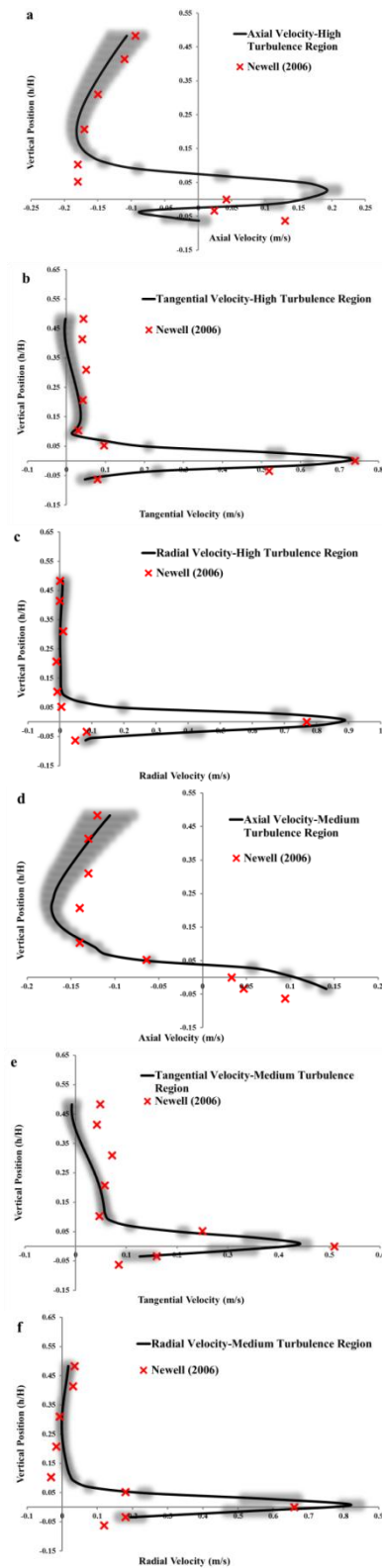


Figure 4: Velocity components as a function of non-dimensional distance from the top of the tank: (a-c) high-turbulent region (26mm from the shaft), (d-f) medium-turbulent region (33mm from the shaft).

Figure 4 shows the numerical predictions of the velocity components as a function of non-dimensional distance

from the top of the tank (h : height, H : tank height) for two regions, close to the impeller and the bulk flow. The solid lines represent the CFD predictions, the symbols correspond to measurements from Newell (Newell, 2006), and the shaded regions illustrate the GCI which was computed using the approach outlined in Methodology section using $p = 1.75$ and $F_s = 1.25$. The figure shows that in all cases the trends in the velocity data as well as the peak tangential and radial velocities at the tip of the impeller have been correctly captured. In addition, the results show that the predicted velocities in the high-turbulent region (i.e., close to the impeller) match the experimental data reasonably well, within an average difference of 26.79% for the axial velocity, 9.13% for the tangential velocity, and 13.29% for the radial velocity. The slightly poor quantitative agreement for the axial velocity in the high-turbulent region can be attributed to the influence of impeller, which causes more axial instability in this region. The predicted velocity components from the medium-turbulent regions (i.e., the bulk flow) are also in a good agreement with the measurements, within an average difference of 16.30% for the axial velocity, 10.61% for the tangential velocity, and 22.78% for the radial velocity.

The shaded regions represent the results of the GCI test which indicate the impact of the numerical uncertainty on the solutions. The overall average of the GCI values for the numerical predictions of the velocity components in the high-turbulent region in the three directions (axial, tangential, and radial) are 13.12%, 12.54%, and 6.80%, respectively, while for the medium-turbulent region these values are 8.19%, 15.86%, and 13.59% for the axial, tangential and radial directions. The relatively small values of GCI for all of the velocity predictions suggest that the numerical uncertainty due to discretization does not significantly influence the numerical solutions. Therefore, the current methodology is capable of accurately simulating the hydrodynamics of the multiphase flow inside the stirred tank. However, the local GCI values for the peak velocity in the tangential and radial directions for the medium-turbulent region (Figure 4-e and f) are fairly large ($GCI < 22.19\%$ for tangential direction and $GCI < 26.12\%$) which suggest that the disagreement between the predictions and simulations in this region could be improved by local mesh refinement.

The under prediction of turbulent quantities has been reported in several studies and has been previously attributed to the lack of a sufficiently fine mesh to accurately resolve the turbulent flow in the stirred tank (Bartels et al., 2002, Lane, 2006, Deglon and Meyer, 2006). To evaluate the discretization error in the numerical predictions of the turbulence, Figure 5 compares the CFD results of the turbulent kinetic energy, k , and the turbulent dissipation rate, ε , to the measurements of Newell. In the figure the solid lines represent the CFD predictions, the symbols correspond to the measurements of Newell (Newell, 2006), and the shaded regions illustrate the computed GCI values. The results show that the trends in the k and ε experimental data have been captured correctly. The maximum turbulent kinetic energy and dissipation rate at the impeller tip are in acceptable agreement with the experimental data (to within an average difference of 29.67% for k and 17.58% for ε). Nevertheless, the moderately high values of GCI at this zone ($GCI < 13.9\%$ for k and $GCI < 17.1\%$ for ε) imply that the local mesh refinement could improve the agreement between the numerical predictions and the experimental

measurements. Although an extremely fine mesh (with 3.7 million cells, Table 1) was used for the prediction of turbulence in this study, the maximum turbulent quantities (i.e., k and ε) have been significantly underpredicted in the bulk flow region. Since the average values of GCI are also small in the medium-turbulent zone ($GCI < 5.4\%$ for k and $GCI < 5.2\%$ for ε), this suggests that the discrepancies between the maximum k and ε with the experimental data could not be minimized by using a more refined mesh. In other words, the quantification of the numerical uncertainty reveals that discretization errors do not contribute significantly to the disagreement between the CFD solution and the experiment. This may therefore indicate that the RANS approach utilizing the standard k - ε turbulence model is unable to accurately predict the turbulent quantities in the stirred tank. One way to tackle this problem might be to use a LES turbulence model, where the large eddies are computed and small eddies are implicitly modelled, instead of a RANS turbulence model, which assumes isotropic turbulence.

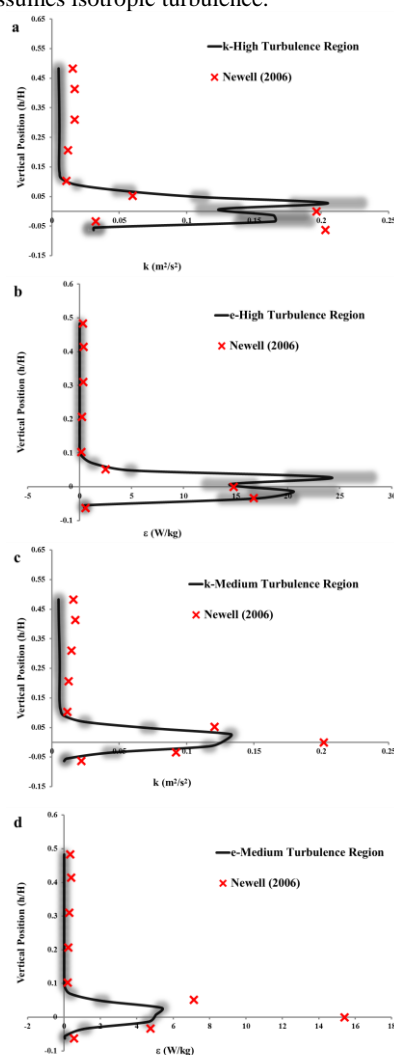


Figure 5: Turbulent kinetic energy (k), and turbulent dissipation rate (ε) as a function of function of non-dimensional distance from the top of the tank (a and b) high-turbulent region (26mm from the shaft), (c and d) medium-turbulent region (33mm from the shaft).

CONCLUSION

The inherent uncertainties in the CFD simulation of a laboratory scale Rushton-turbine flotation tank were quantified in this study. An Eulerian-Eulerian multiphase model in conjunction with the dispersed k - ϵ turbulence model was applied to predict the velocity components and the gas holdup. To reduce the influence of the model uncertainties in the CFD predictions of the gas holdup different sparger designs at various locations with respect to the impeller position were implemented. The results showed that the sparger design significantly varies the gas holdup predictions and the optimized design of sparger can reduce the uncertainty due to the model implementation. Numerical uncertainty due to discretization error was evaluated using the Grid Convergence Index (GCI). The results of the GCI test showed that the CFD model applied in this study was able to produce reasonable predictions of the flow inside the stirred tank. However, the slightly high values of GCI for peak velocities in the tangential and radial directions in the bulk flow region indicate that local mesh refinement will yield better agreement between simulation and experiment. The numerical predictions of maximum turbulent quantities (k and ϵ) showed an acceptable agreement (to within an average difference of 29.67% for k and 17.58% for ϵ) in the high-turbulence region and the fairly large values of GCI (GCI<13.9% for k and GCI<17.1% for ϵ) in the impeller region confirmed that the turbulence predictions might be closer to the experimental data by refining the mesh in this zone. The GCI test yielded interesting results for the numerical predictions of k and ϵ for the bulk flow. The small values of GCI (GCI<5.4% for k and GCI<5.2% for ϵ) for this region revealed that the observed under prediction of the turbulence parameters could not be improved by refining the mesh owing to the insignificant effects of discretization error. Overall the results suggest that quantification of uncertainties in CFD simulations can lead to improved predictions of the gas holdup and flow dynamics in a laboratory scale Rushton-turbine tank.

ACKNOWLEDGMENT

This work was supported by OSP funding from Stellenbosch University in South Africa.

REFERENCES

BARTELS, C., BREUER, M., WECHSLER, K. and DURST, F., (2002), "Computational fluid dynamics applications on parallel-vector computers: computations of stirred vessel flows", *Computers & Fluids*, **31**, 69-97.

CORONEO, M., MONTANTE, G., PAGLIANTI, A. and MAGELLI, F., (2011), "CFD prediction of fluid flow and mixing in stirred tanks: Numerical issues about the RANS simulations", *Computers & Chemical Engineering*, **35**, 1959-1968.

DEGLON, D. A. and MEYER, C. J., (2006), "CFD modelling of stirred tanks: Numerical considerations", *Minerals Engineering*, **19**, 1059-1068.

DONG, L., JOHANSEN, S. T. and ENGH, T. A., (1994a), "Flow induced by an impeller in an unbaffled tank—I. Experimental", *Chemical Engineering Science*, **49**, 549-560.

DONG, L., JOHANSEN, S. T. and ENGH, T. A., (1994b), "Flow induced by an impeller in an unbaffled tank—II. Numerical modelling", *Chemical Engineering Science*, **49**, 3511-3518.

FINCH, J. A., XIAO, J., HARDIE, C. and GOMEZ, C. O., (2000), "Gas dispersion properties: bubble surface area flux and gas holdup", *Minerals Engineering*, **13**, 365-372.

FREITAS, C. J., (2002), "The issue of numerical uncertainty", *Applied Mathematical Modelling*, **26**, 237-248.

KARIMI, M., AKDOGAN, G. and BRADSHAW, S. M., (2012), "Effects of different mesh schemes and turbulence models in CFD modelling of stirred tanks", *Physicochemical Problems of Mineral Processing*, **48**, 513-531.

KERDOUSS, F., BANNARI, A. and PROULX, P., (2006), "CFD modeling of gas dispersion and bubble size in a double turbine stirred tank", *Chemical Engineering Science*, **61**, 3313-3322.

KHOPKAR, A. R., KASAT, G. R., PANDIT, A. B. and RANADEV, V. V., (2006), "CFD simulation of mixing in tall gas-liquid stirred vessel: Role of local flow patterns", *Chemical Engineering Science*, **61**, 2921-2929.

LANE, G. L., (2006), "Computational Modelling of Gas-Liquid Flow in Stirred Tanks", PhD, University of Newcastle, Australia.

LANE, G. L., SCHWARZ, M. P. and EVANS, G. M., (2000), "Comparison of CFD methods for modelling of stirred tanks", *10th European Conference on Mixing*, Delf, Netherlands, 273-280.

LANE, G. L., SCHWARZ, M. P. and EVANS, G. M., (2002), "Predicting gas-liquid flow in a mechanically stirred tank", *Applied Math. Modelling*, **26**, 223-235.

LANE, G. L., SCHWARZ, M. P. and EVANS, G. M., (2005), "Numerical modelling of gas-liquid flow in stirred tanks", *Chemical Engineering Science*, **60**, 2203-2214.

NEWELL, R., (2006), "Hydrodynamics and scale-up in rushton turbine flotation cells", PhD, University of South Australia.

NEWELL, R. and GRANO, S., (2007), "Hydrodynamics and scale up in Rushton turbine flotation cells: Part 1 — Cell hydrodynamics", *International Journal of Mineral Processing*, **81**, 224-236.

OSHINOWO, L., JAWORSKI, Z., DYSTER, K. N., MARSHALL, E. and NIENOW, A. W., (2000), "Predicting the tangential velocity field in stirred tanks using the multiple reference frames (MRF) Model with validation by LDA measurements", *10th European Conference on Mixing*, Delf, Netherland, 281-288.

RICHARDSON, L. F., (1911), "The Approximate Arithmetical Solution by Finite Differences of Physical Problems Involving Differential Equations, with an Application to the Stresses in a Masonry Dam", *Philosophical Transactions of the Royal Society of London. Series A, Containing Papers of a Mathematical or Physical Character*, **210**, 307-357.

RICHARDSON, L. F. and GAUNT, J. A., (1927), "The Deferred Approach to the Limit. Part I. Single Lattice. Part II. Interpenetrating Lattices", *Philosophical Transactions of the Royal Society of London. Series A, Containing Papers of a Mathematical or Physical Character*, **226**, 299-361.

ROACHE, P. J., (1994), "Perspective: A method for uniform reporting of grid refinement studies", *Journal of Fluids Engineering*, **116**, 405-413.

SCHILLER, L. and NAUMANN, Z., (1935), Ver. Deutsch Ing.

SENSEL, M. E., MYERS, K. J. and FASANO, J. B., (1992), "Gas dispersion at high aeration rates in low to moderately viscous Newtonian liquids", AICHE Annual Meeting, Miami Beach, Florida, 76-84.

APPENDIX 1.

Type	ds/D*	Simulation		Experiments	
		Angular Velocity (rpm)	Gas-Holdup (%)	Angular Velocity (rpm)	Gas-Holdup (%)
Ring	0.5	350	4.33	350	5.2
Ring	0.5	0	4.44	0	3.7
Ring	0.75	350	4.81	350	5.2
Ring	0.75	0	5.08	0	3.7
Ring	1	350	5.63	350	5.2
Ring	1	0	5.61	0	3.7
Disk	0.4	350	6.86	350	5.2
Disk	0.4	0	4.00	0	3.7
Disk	0.5	350	14.56	350	5.2
Disk	0.5	0	6.12	0	3.7
Disk	0.75	350	36.64	350	5.2
Disk	0.75	0	16.56	0	3.7

Table A.1: Summarization of the different sparger diameters for two types of design (ds: sparger diameter, D: impeller diameter).

Type	ds/D	Location	Simulation		Experiments	
			Angular Velocity (rpm)	Gas-Holdup (%)	Angular Velocity (rpm)	Gas-Holdup (%)
Ring	0.5	bottom	350	4.33	350	5.2
			0	4.44	0	3.7
		middle of clearance	350	2.55	350	5.2
			0	2.62	0	3.7
		close to the impeller	350	2.24	350	5.2
			0	1.80	0	3.7
Disk	0.4	bottom	350	6.86	350	5.2
			0	4.00	0	3.7
		middle of clearance	0	6.41	350	5.2
			0	3.81	0	3.7
		close to the impeller	350	5.28	350	5.2
			0	3.05	0	3.7

Table A.2: Simulations for different sparger locations.